ACCEPTED MANUSCRIPT

The Journal of Chemical Physics

AIP Publishing

This is the author's peer reviewed, accepted manuscript. However, the online version of record will be different from this version once it has been copyedited and typeset.
PLEASE CITE THIS ARTICLE AS DOI: 10.1063/5.0144851

Unravelling the decarboxylation dynamics of the fluorescein dianion with fragment action spectroscopy

Jemma A. Gibbard and Jan R. R. Verlet*

Department of Chemistry, Durham University, Durham DH1 3LE, United Kingdom

**Email: jemma.gibbard@durham.ac.uk*

Abstract

The decarboxylation dynamics of the doubly deprotonated fluorescein dianion, Fl^{2-}, are investigated by recording fragment action spectra for the anion, Fl^-, and its decarboxylated analogue, $Fl\text{-}CO_2^-$, using a new reflectron secondary mass spectrometer. The formation of the anion, Fl^-, is directly investigated by photoelectron imaging. The Fl^- and $Fl\text{-}CO_2^-$ action spectra indicate that, for λ < 400 nm, one-photon dissociative photodetachment, i.e. simultanous decarboxylation and electron loss, competes with photodetachment, whereas for λ > 400 nm, decarboxylation only proceeeds following electron loss via a sequential two-photon process. The primary decarboxylation pathway is the ready loss of CO_2 from the relatively short-lived intermediate excited state, $Fl^-[D_1]$, which is formed by electron loss from the dianion via resonant tunnelling through the repulsive Coloumb barrier associated with a high-lying excited dianion state, $Fl^{2-}[S_2]$.

ACCEPTED MANUSCRIPT
The Journal of Chemical Physics
AIP Publishing
This is the author's peer reviewed, accepted manuscript. However, the online version of record will be different from this version once it has been copyedited and typeset.
PLEASE CITE THIS ARTICLE AS DOI: 10.1063/5.0144851

I. Introduction

Fluorescein is a dye and fluorescent tracer, where many of its applications exploit its intense solution-phase fluorescence.[1] Several charged and neutral pH dependent forms of fluorescein exist in the solution phase, including a doubly deprotonated dianion (Fl^{2-}), which has a fluorescence maximum at 500 nm, corresponding to radiative relaxation from $S_1 \rightarrow S_0$.[1, 2] While the fluorescence quantum yield in solution is very high, previous studies have indicated that Fl^{2-} does not fluoresce in the gas phase; instead, S_1 decays via electron loss.[2, 3] Decarboxylation of the carboxylate group of Fl^{2-} may also be favourable, given the high thermodynamic stability of CO_2, particuarly if the Fl^- radical anion that is formed following electron loss from the dianion has carboxyl radical character.[4, 5] In fact, multiple photon excitation of Fl^{2-} in the IR (via irradiation with a CO_2 laser) and collisionally induced dissociation (CID) of Fl^{2-} was found to exclusively produce decarboxylation with electron loss (i.e. $Fl\text{-}CO_2^- + e^- + CO_2$), in contrast to excitation in the visable, where electron loss was the dominant channel (i.e. $Fl^- + e^-$).[2] Therefore, the mechanism for decarboxylation, as well as the role of excited states in mediating the electron loss and decarboxylation dynamics of Fl^{2-}, remains unclear. In this manuscript we present fragment action spectroscopy of Fl^{2-} in the gas-phase between $\lambda = 260 - 600$ nm in order to gain insight into the competition between electron and CO_2 loss from Fl^{2-}.

Dianions, such as Fl^{2-}, are characterised by the balance of long range repulsive forces and short range attractive forces, which constitute the repulsive Coulomb barrier (RCB).[3, 6-11] There are a multitude of RCBs associated with a dianion corresponding to individual rovibronic states of the parent species and linked to distinct product channels, whether that be electron or anion loss channels.[12, 13] Therefore each RCB forms a barrier to the loss of low kinetic energy electrons or anionic fragments. One key distinction between the study of electron loss and anionic dissociation processes of dianions is the relative prevalence of tunnelling through a

ACCEPTED MANUSCRIPT
The Journal of Chemical Physics
AIP Publishing
This is the author's peer reviewed, accepted manuscript. However, the online version of record will be different from this version once it has been copyedited and typeset.
PLEASE CITE THIS ARTICLE AS DOI: 10.1063/5.0144851

specific RCB. Resonant and non-resonant electron tunnelling through an RCB has been observed for many dianions, on account of the low mass of the electron.[14-17] In contrast, anionic fragmentation of dianions has only been observed as an 'over-the-barrier' process.[13, 18]

Experimentally, the properties of dianions and their electronic RCBs have been effectively studied by photoelectron spectroscopy, where a characteristic low electron kinetic energy (eKE) cutoff is observed in the photoelectron spectra at the minimum height of the RCB.[18-22] Electron loss via tunnelling has been observed by the prescence of photoelectrons below the cutoff, and these features are often spectrally characterised by a peak at fixed eKE, which is invariant with photon energy.[3, 12, 23] Photodissociation spectroscopy has also been used to study anion loss from dianions, in particular for $IrBr_6^{2-}$, where the minimum height of the RCB to fragmentation has been reported from the kinetic energy release of the Br^- fragment.[13, 18, 24, 25] The groups of Weber and Kappes have used reflectron time-of-flight mass spectrometry to record fragment action spectra,[18, 25, 26] whilst other methodologies, such as the collisional activation or laser excitation of dianions in a quadrupole trap or electrostatic ion storage rings, have also been used to study polyanion dissociation dynamics.[2, 13, 24]

Previous work in our group has studied the photodetachment dynamics of Fl^{2-} using frequency-resolved photoelectron imaging.[3, 12, 27] Unusual and rich photodetachment dynamics were observed, with electron loss occuring via several distinct resonant tunnelling pathways that are associated with different mediating dianion states, RCBs and final anion states.[12] While photoelectron spectroscopy can yield a detailed picture of the electron loss dynamics, once the electron has been lost, this methodology is blind to any subsequent dynamical process, such as dissociation. This is the case for Fl^{2-}, where CO_2 loss has been observed in conjunction with electron loss under specific experimental circumstances.[2] So how do such dissociation dynamics take place and can this be reconciled with the electron dynamics? Commonly observed processes involve electron loss from a carboxylate anion leading to rapid

ACCEPTED MANUSCRIPT
The Journal of Chemical Physics
AIP Publishing
This is the author's peer reviewed, accepted manuscript. However, the online version of record will be different from this version once it has been copyedited and typeset.
PLEASE CITE THIS ARTICLE AS DOI: 10.1063/5.0144851

decarboxylation of a transiently formed carboxyl radical via a repulsive potential energy surface.[4, 5, 28-30] However it is unclear if the Fl^- formed following electron loss from Fl^{2-} would have carboxyl radical character and be expected to undergo a similar repulsive dissociation. Additionally, the photodetachment dynamics indicate that at higher photon energies, new tunnelling pathways compete that lead to the formation of a highly internally excited Fl^-, both electronic and/or vibrational. The role of vibrational excitation may be important if CO_2 loss occurs via a ground state dissociation, while different electronic states in the anionic product may have different dissociation dynamics. In this manuscript we build on the previously reported photoelectron imaging studies, which focused on the nature of the RCB, to unravel the decarboxylation dynamics of Fl^{2-} by the application of fragment action spectroscopy.[3, 12]

II. Methods

The action spectrum of a fragment ion cannot be recorded using linear time-of-flight methods as, to a first approximation, all of the photoproducts have the same velocity as the parent species, making it challenging to separate the time-of-flight of the fragment ions from the parent dianions. In order to overcome this limitiation, a secondary mass spectrometer consisting of a reflectron was introduced, which acts as an electrostatic kinetic energy filter, in order to temporally separate the charged photoproducts with different $\frac{m}{z}$ ratios.[31, 32] We can study both the photodetachment (different z) and photodissociation (different m and sometimes z) of dianions using this methodology.

The ion beam and light source used in this apparatus are the same as for previous photoelectron imaging experiments and have been described in detail elsewhere.[33, 34] Briefly Fl^{2-} was produced using electrospray ionization of a 1 mM solution of sodium fluorescein in methanol. The dianions entered the vacuum via a capillary and were guided and trapped by a series of radiofrequency ring electrodes, before acceleration at -1.5 keV using a Wiley-

ACCEPTED MANUSCRIPT
The Journal of Chemical Physics
AIP Publishing
This is the author's peer reviewed, accepted manuscript. However, the online version of record will be different from this version once it has been copyedited and typeset.
PLEASE CITE THIS ARTICLE AS DOI: 10.1063/5.0144851

Maclaren time-of-flight mass spectrometer. The dianions of interest were mass selected by time-of-flight at the intersection of the ion beam with the nanosecond tuneable output of a Nd:YAG pumped optical parametric oscillator, which induces photochemistry in Fl^{2-}. Likely photoproducts include photoelectrons, which can be studied by photoelectron imaging,[19, 20] and anions produced via electron loss, dissociation or a combination of both.

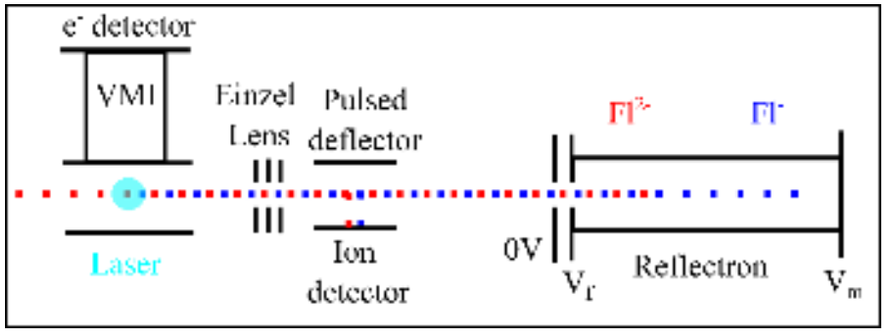

Figure 1: Schematic of the new detector region including the electron detector, reflectron secondary mass spectrometer and pulsed ion detection scheme, as used for the experiments on Fl^{2-}. The shorter flight path of Fl^{2-} ($\frac{m}{z} = 165\ amu$), produced via electrospray ionization and mass selected from its time-of-flight, is represented by the red dots, whereas the longer flight path of Fl^{-} ($\frac{m}{z} = 330\ amu$) is shown by the blue dots.

The new detector region, including the reflectron secondary mass spectrometer, is shown schematically in Figure 1. After the interaction of laser light and Fl^{2-}, any product anions, including Fl^{-} (blue), continue along the same beam axis as Fl^{2-} (red), past a grounded detector and deflector, and into the reflectron. As the kinetic energy of the dianion ($\frac{m}{z} = \frac{m_{Fl}}{2} = 165$ amu) is half that of the anion ($\frac{m}{z} = m_{Fl} = 330$ amu), the two ion packets can be temporally seperated by the behaviour of the reflectron as a kinetic energy filter. The reflectron consists of a grounded front plate, followed by a resistive glass tube (15 cm long) that is biased at either end (front plate, V_f = -700 V and mirror plate, V_m = - 3500 V). As the kinetic energy of the anion product is twice as large as the dianion, the mirror voltage of the reflectron must be more than twice the beam energy of the dianion in order to reflect the anions for detection. This is shown in Figure 1 by the Fl^{2-} (red) and Fl^{-} (blue) ion paths, where the flight distance is

ACCEPTED MANUSCRIPT
The Journal of Chemical Physics
AIP Publishing
This is the author's peer reviewed, accepted manuscript. However, the online version of record will be different from this version once it has been copyedited and typeset.
PLEASE CITE THIS ARTICLE AS DOI: 10.1063/5.0144851

substantially longer for the species with larger kinetic energy. Typically, reflectrons consist of a stack of metal plates linked via a chain of resistors,[18, 31] but the use of a restistive glass tube here allows the reflectron to act as an infinite chain of electrodes. This minimises lensing and fringe field effects near individual electrodes, in order to maximise the fragment mass resolution of the reflectron, whilst maintaining its short length. Similar resistive glass tubes have been used in the velocity map imaging of electrons.[33] Once the ions enter the reflectron, the deflector is pulsed (from 0 V to -3 kV, pulse duration ~100 μs) to push anions (parent dianions and fragment anions) into the ion detector on the second pass, so that the time-of-flight of each species can be recorded.

If any additional anionic photoproducts are formed following irradiation with laser light, then additional peaks will be observed in the secondary mass spectra. For example, Fl-CO_2^- has a time of flight between Fl^{2-} and Fl^- ($\frac{m}{z} = \frac{330-44}{1} = 286$ amu). Generally, ion peaks are assigned to a specific $\frac{m}{z}$ by comparison of the experimental ion arrival times to the results of a simple model, which calculates the acceleration of an ion of a specific $\frac{m}{z}$ within the applied fields, extracts an ion turn around position and ultimately predicts a time-of-flight.

Following assignment of the species in the secondary mass spectrum, action spectra can be recorded by monitoring the intensity of the signal from a specific mass-selected species, as a function of laser wavelength. The laser was scanned at a rate of 0.1 nm s^{-1} and scans were repeated three times. All of the ion peak intensities in the following action spectra were normalised to the integral of the parent dianion peak in order to account for substantial fluctuations in the parent ion beam. The low intensity of the fragment signal requires additional amplification after the detector, resulting in saturation of the Fl^{2-} ion signal on the final time-of-flight trace (Figure SI1). However, the effect of this on the reported action spectra is minimal, as the Fl^{2-} ion intensity was very constant, as verified by measurement of the parent ion signal without further amplification, and by repeated measurements of the action spectra which were

ACCEPTED MANUSCRIPT

The Journal of Chemical Physics

AIP Publishing

This is the author's peer reviewed, accepted manuscript. However, the online version of record will be different from this version once it has been copyedited and typeset.
PLEASE CITE THIS ARTICLE AS DOI: 10.1063/5.0144851

very similar. We are currently modifying the data acquisition setup to allow us to independently amplify the fragment signal, which should result in a more sensitive normalisation procedure in the future. It should also be noted that no attempt has been made to account for the significant changes in laser intensity which occur over this wavelength range, with particular minima being observed at 400 nm and 292 nm, that are characteristic of our optical parametric oscillator, while over other regions, the output was found to be relatively constant in terms of pulse energy. Electron yield spectra can also be acquired by simply monitoring the number of electrons on the imaging detector as a function of wavelength.

To aid interpretation of the results, additional electronic structure calculations were performed on Fl^{2-}, Fl^{-} and $Fl\text{-}CO_2^{-}$. Ground state density functional theory (DFT) calculations and excited state time-dependent DFT calculations, using the Tamm-Dancoff approximation, were performed using the Gaussian software package at the B3LYP level of theory with the 6-311G ++ 2d,2p basis set.[35-37]

III. Results and Analysis

In the absence of laser light, the secondary mass spectrum consisted of a single peak with $\frac{m}{z}$ = 165 amu, assignable to Fl^{2-}. Once the sample was irradiated, two further peaks were observed over specific wavelength ranges, corresponding to $Fl\text{-}CO_2^{-}$ and Fl^{2-}. An example time-of-flight spectrum is shown in the supplementary information, Figure SI1. No evidence was seen for the formation of other products such as $Fl\text{-}CO_2^{2-}$, indicating that dissociation only occurred in conjunction with electron loss.

A. Photoelectron imaging of Fl^{2-}

ACCEPTED MANUSCRIPT
The Journal of Chemical Physics
AIP Publishing
This is the author's peer reviewed, accepted manuscript. However, the online version of record will be different from this version once it has been copyedited and typeset.
PLEASE CITE THIS ARTICLE AS DOI: 10.1063/5.0144851

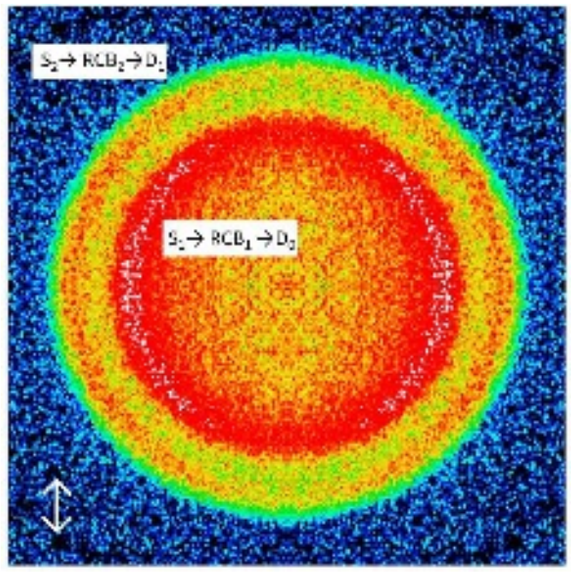

Figure 2: Raw (symmetrised) photoelectron image of Fl^{2-} recorded at $\lambda = 320$ nm with the polarisation vector of the light shown by the double arrow.

Previous work in our group has studied the photodetachment dynamics of Fl^{2-} using frequency resolved photoelectron imaging.[3, 12, 27] A brief overview of this work is presented here as its conclusions will guide some of the discussion below. Figure 2 shows the Fl^{2-} photoelectron image recorded at $\lambda = 320$ nm, where two clear spectral features are observed. Photoelectron imaging in the visible reported a single fixed eKE feature, which remains even in the UV and corresponds to the inner ring in Figure 2. This feature arises from resonant tunnelling through an RCB associated with the $Fl^{2-}[S_1]$ state (RCB_1).[3] As this feature's eKE is fixed with decreasing λ, the excess photon energy following electron loss will be deposited as internal rovibrational energy in the ground-state anion, $Fl^{-}[D_0]$.[3] For UV excitation, a second higher-lying and competing tunnelling pathway (outer ring in Figure 2) appears following excitation to the S_2 state of Fl^{2-}, $Fl^{2-}[S_2]$. A fraction of the population tunnels through a RCB associated with the S_2 state, RCB_2, resulting in a different final anion electronic state, $Fl^{-}[D_1]$.[12] The different final states accessed by tunnelling arise from different Koopmans' correlations.[12] At wavelengths in the visible ($\lambda \leqslant 540$ nm) only the inner feature is observed in the

ACCEPTED MANUSCRIPT
The Journal of Chemical Physics
AIP Publishing
This is the author's peer reviewed, accepted manuscript. However, the online version of record will be different from this version once it has been copyedited and typeset.
PLEASE CITE THIS ARTICLE AS DOI: 10.1063/5.0144851

photoelectron images, whereas the outer ring competes at higher photon energies in the UV ($\lambda \leqslant 350$ nm). In addition, a minor direct detachment channel was observed for $\lambda \leqslant 440$ nm, at electron kinetic energies which overlapped with the resonant tunnelling pathway mediated by S_2 (outer ring).

B. Action spectra of Fl^{2-}: fragment and electron yield

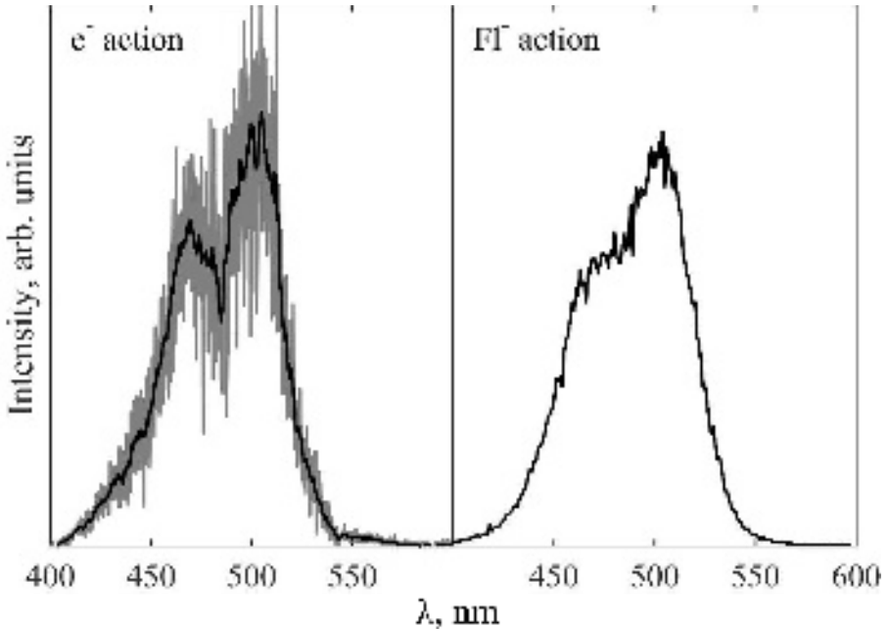

Figure 3: Comparison of the action spectra of Fl^{2-} recorded by monitoring the electron yield on the left (grey and a 20-point moving average in black) and the Fl^- yield on the right in black.

In order to confirm the functionality of the new reflectron, the action spectra of both the electron and Fl^- yield arising from photodetachment of Fl^{2-} were recorded at wavelengths between 400 nm and 600 nm, and are shown in black in Figure 3. The electron action spectrum is smoothed via a 20-point moving average, with the raw data shown in grey. The electron and Fl^- action spectra are similar in structure, indicating that the primary process following absorption of a photon is a one-photon photodetachment to form the radical anion i.e. $Fl^{2-} \rightarrow$

ACCEPTED MANUSCRIPT
The Journal of Chemical Physics
AIP Publishing
This is the author's peer reviewed, accepted manuscript. However, the online version of record will be different from this version once it has been copyedited and typeset.
PLEASE CITE THIS ARTICLE AS DOI: 10.1063/5.0144851

$Fl^- + e^-$, in agreement with previous work.[2, 3] The small differences between the electron and the Fl^- yield spectra, shown in black, are likely to be within the noise of the two measurements, or attributable to the two spectra being recorded with different detectors.

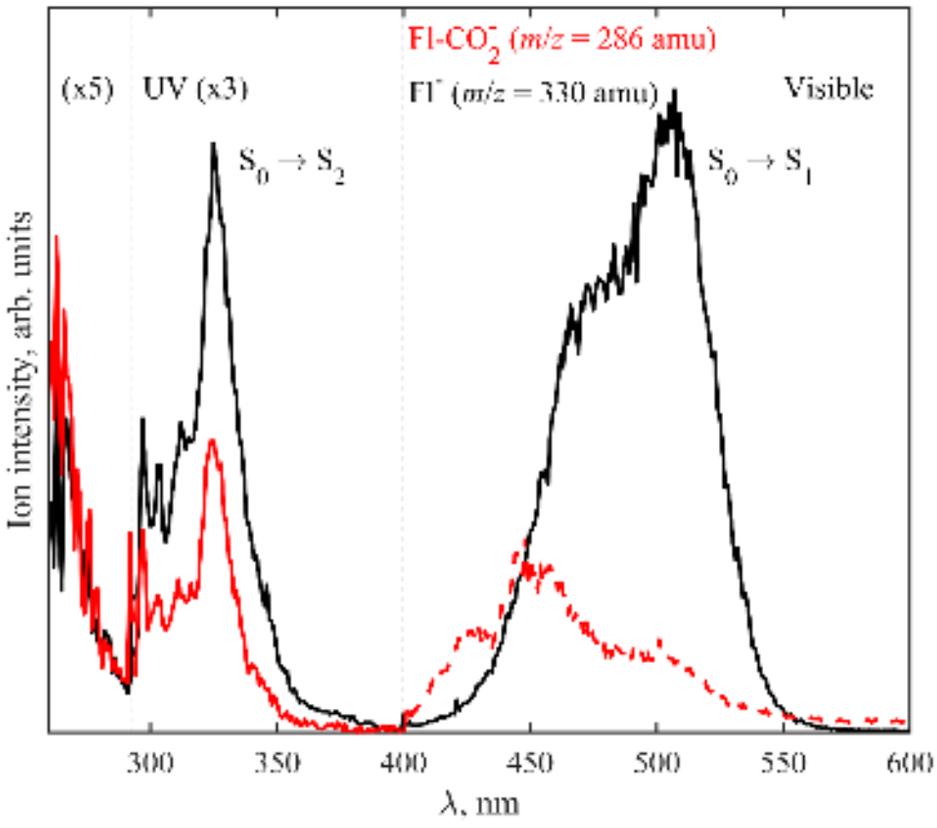

Figure 4: The action spectra of Fl^{2-} obtained by monitoring the fragments Fl^- (black) and Fl-CO_2^- (red). All the processes are one-photon, except for the dashed line which arises from a multiple photon process (see text for more details). The vertical dashed lines indicate three different spectral ranges of the light source and the relative intensities on either side of these lines are not representative of the true intensity.

The black line in Figure 4 is the action spectrum of Fl^{2-} recorded over a wider wavelength range, $\lambda = 260 – 600$ nm, by monitoring the Fl^- fragment. This action spectrum has a similar structure to the previously reported gas-phase action spectrum of Fl^{2-} and the absorption spectrum of Fl^{2-} in water at $\lambda > 400$ nm, indicating that the regions of increased signal intensity are due to the presence of an increased photodetachment cross-section for Fl^{2-}, *i.e.* the location of an excited electronic state.[1, 2] The most intense feature is centred around 500

ACCEPTED MANUSCRIPT
The Journal of Chemical Physics
AIP Publishing
This is the author's peer reviewed, accepted manuscript. However, the online version of record will be different from this version once it has been copyedited and typeset.
PLEASE CITE THIS ARTICLE AS DOI: 10.1063/5.0144851

nm and corresponds to the bright $S_0 \rightarrow S_1$ transition in Fl^{2-}. This feature shows some vibrational structure, similar to the solution phase absorption spectrum. Irradiation of Fl^{2-} near 400 nm produces very little Fl^-, indicating that the photodetachment cross-section is very low in this region, even though at this wavelength, direct 'over-the-RCB' detachment is an open channel.[3, 12] At higher photon energies an increased yield of Fl^- is observed, as higher-lying electronic states of Fl^{2-} become energetically accessible. In particular S_2 is located near 325 nm, with potential evidence for S_3 at $\lambda < 292$ nm. It should be noted that a portion of this action spectrum ($\lambda = 300 - 600$ nm) has been published before.[12]

C. Action spectrum of Fl^{2-}: Fl-CO_2^- yield

The action spectrum of the decarboxylated anion Fl-CO_2^- was also recorded using the reflectron and is shown in red in Figure 4. The Fl-CO_2^- action spectrum is similar in appearance to Fl^- at wavelengths shorter than 400 nm (solid red line), but significantly different at longer wavelengths (dashed red line). The excellent correlation between the Fl-CO_2^- and Fl^- yield spectra for $300 < \lambda < 400$ nm indicates that a one-photon process can either lead to just electron loss *or* combined electron and CO_2 loss, with the former being approximately twice as likely around the S_2 excited state.

In the visible range, the discrepancy between the Fl-CO_2^- and Fl^- yield spectra is due to a multiple photon process, which can be evidenced by the action spectrum taken at lower laser power. As the formation of Fl^- is a one-photon process, differences in the relative intensity of the Fl-CO_2^- peak, would indicate a multiple photon process. Figure SI2 shows the Fl^{2-} action spectra recorded by monitoring the Fl^- and Fl-CO_2^- yields at wavelengths between 400 and 500 nm and at a third of the laser power used for the measurement in Figure 4. Based on the large decrease in the relative intensity of Fl-CO_2^- compared to Fl^- from Figure 4 to SI2, we conclude that the formation of Fl-CO_2^- at $\lambda > 400$ nm occurs via a multiple photon process, presumably

a two-photon process (dashed red line). The formation of Fl^- at all wavelengths and $Fl\text{-}CO_2^-$ for $\lambda < 400$ nm is a one-photon process (solid red line).

D. Action spectrum of Fl^-

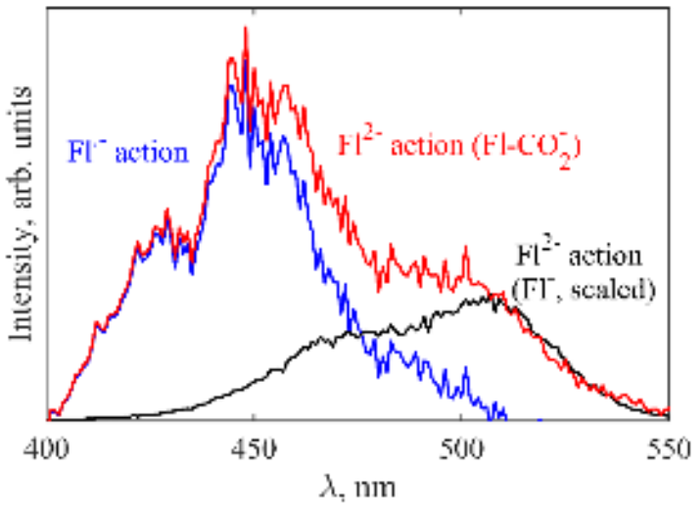

Figure 5: Action spectrum of the Fl^- radical anion (blue), extracted from action spectra of Fl^{2-} by taking the difference of the $Fl\text{-}CO_2^-$ (red) and the scaled Fl^- (black) yield spectra.

The power dependent measurements suggest that electron loss and decarboxylation occur stepwise via a two-photon process at wavelengths longer than 400 nm ($h\nu < 3.1$ eV):

$$Fl^{2-} \xrightarrow{h\nu < 3.1\ eV} Fl^- + e^-$$

$$Fl^- \xrightarrow{h\nu < 3.1\ eV} Fl\text{-}CO_2^- + CO_2$$

The second step corresponds to the action spectrum of the radical anion Fl^-, rather than the parent dianion. Hence, the total measured action spectrum of Fl^{2-} by monitoring the $Fl\text{-}CO_2^-$ fragment (red line in Figure 4) across the visible contains both steps. By scaling the Fl^- yield spectrum to fit the red-edge of the $Fl\text{-}CO_2^-$ yield spectrum, and subsequently taking their

ACCEPTED MANUSCRIPT
The Journal of Chemical Physics
AIP Publishing
This is the author's peer reviewed, accepted manuscript. However, the online version of record will be different from this version once it has been copyedited and typeset.
PLEASE CITE THIS ARTICLE AS DOI: 10.1063/5.0144851

ACCEPTED MANUSCRIPT
The Journal of Chemical Physics
AIP Publishing
This is the author's peer reviewed, accepted manuscript. However, the online version of record will be different from this version once it has been copyedited and typeset.
PLEASE CITE THIS ARTICLE AS DOI: 10.1063/5.0144851

difference, it is possible to extract the $Fl^-[D_0]$ action spectrum. The action spectrum of Fl^- (blue), as well as the scaled versions of the Fl^- (black) and Fl-CO_2^- (red) yield spectra are shown in Figure 5. The action spectrum of Fl^- is similar in structure to the action spectrum of Fl^{2-} in Figure 4 (black) but shifted to higher energy. Note also that three peaks are seen with a similar spacing (~ 0.15 eV), suggesting they correspond to the vibrational manifold of the $Fl^-[S_1]$ excited state. The low intensity of the lowest energy peak is indicative that this feature may correspond to a hot band, which is unsurprising given the likely presence of significant internal excitation in the anion following electron loss.[3]

IV. Discussion

Decarboxylation is a common process in carboxylates and carboxyl radicals, driven by the large thermodynamic stability of CO_2.[4, 5, 38-40] It has been observed to occur via a photodissociation or dissociative photodetachment (DPD) process in carboxylate anions, and even via secondary dissociative autodetachment in dicarboxylate dianions.[4, 5, 40] In the case of combined electron and CO_2 loss, as observed for Fl^{2-}, it is likely that electron loss and CO_2 loss occur sequentially, rather than via the formation of CO_2^-, given that CO_2 has a negative electron affinity.[41] Therefore the mechanism for decarboxylation of Fl^{2-} is likely to be either DPD ($Fl^{2-} \xrightarrow{h\nu} Fl^- + CO_2 + e^-$), which may occur via a repulsive electronic state of the Fl^- anion, e.g. $Fl^-[D_1]$, or via the formation of a vibrationally excited $Fl^-[D_0]$, that then undergoes unimolecular dissociation, or a combination of these processes on different anionic electronic states.

As electron loss is the first step in the formation of both Fl^- and Fl-CO_2^-, the photoelectron imaging of Fl^{2-} (e.g. Figure 2) will inform on the electron loss processes that lead to specific fragments at a given wavelength (Figure 4).[3, 12] Two resonant electron loss processes have been observed: (1) resonant tunnelling through RCB_1 from the $Fl^{2-}[S_1]$ to $Fl^-[D_0]$ at all wavelengths studied (300 nm $\leq \lambda \leq$ 540 nm); and (2) a second resonant tunnelling channel

ACCEPTED MANUSCRIPT
The Journal of Chemical Physics
AIP Publishing
This is the author's peer reviewed, accepted manuscript. However, the online version of record will be different from this version once it has been copyedited and typeset.
PLEASE CITE THIS ARTICLE AS DOI: 10.1063/5.0144851

through RCB_2 from $Fl^{2-}[S_2]$ to $Fl^-[D_1]$ at $\lambda < 350$ nm.[3, 12] For $\lambda < 350$ nm, both processes compete as both are visible in the photoelectron image (Figure 2).[12] There is a third electron loss channel due to detachment to $Fl^-[D_0]$ over RCB_0 (linking $Fl^{2-}[S_1]$ and $Fl^-[D_0]$) occurring at $\lambda \leq 440$ nm.[3, 42] However, this is a very minor channel as evidenced by the low Fl^- ion signal observed at non-resonant wavelengths ($350 \text{ nm} \leq \lambda \leq 440$ nm).[12]

At the longest wavelengths studied ($440 \leq \lambda \leq 600$ nm) absorption of a single photon populates the excited dianion state, $Fl^{2-}[S_1]$ and the only available channel is electron tunnelling through RCB_1 to form a $Fl^-[D_0]$,[3] with no decarboxylation. The final anionic product $Fl^-[D_0]$, while internally hot, is stable on a timescale longer than the flight time (~20 μs) as it is observed in the fragment action spectra (Figure 4).[3] At shorter wavelengths ($\lambda \leq 350$ nm), where the two resonant electron loss channels compete, there is ion intensity in the Fl^- and $Fl\text{-}CO_2^-$ yield spectra (Figure 4) in a ratio of ~2:1, indicating a competition between photodetachment and DPD following one-photon excitation of Fl^{2-}. One explanation is that $Fl^-[D_1]$ is a repulsive electronic state, whereas $Fl^-[D_0]$ is bound, such that CO_2 loss occurs readily following the formation of $Fl^-[D_1]$, whereas $Fl^-[D_0]$ is stable on the timescale of the experiment i.e. the flight time from the interaction region to the turnaround point in the reflectron. Evidence for $Fl\text{-}CO_2^-$ formation via a repulsive dissociation is found in the comparable width of the $Fl\text{-}CO_2^-$ and Fl^- peaks in the time-of-flight spectrum (Figure SI1). This indicates that the timescale of decarboxylation is shorter than the flight time from the interaction region to the reflectron (~5 μs), because if dissociation occurred within the reflectron itself, a much broader distribution of ion arrival times would be expected. Hence, the DPD process appears to be prompt rather than statistical in nature.

Table 1: Relative energetics of Fl^{2-}, Fl^- and $Fl\text{-}CO_2^-$ in various electronic states. Vertical excitation and detachment energies are labelled VEE and VDE respectively. Values labelled with an asterisk have been reported previously.[12]

Species [electronic state]	Relative Energy (eV)

ACCEPTED MANUSCRIPT

The Journal of Chemical Physics

AIP Publishing

This is the author's peer reviewed, accepted manuscript. However, the online version of record will be different from this version once it has been copyedited and typeset.
PLEASE CITE THIS ARTICLE AS DOI: 10.1063/5.0144851

$Fl^{2-}[S_0]$	0*
$Fl^{-}[D_0]$	0.62 (0.74 VDE)*
$Fl^{-}[D_1]$	1.35 (VEE)*
$Fl\text{-}CO_2^{-}[D_0] + CO_2$	1.44
$Fl^{2-}[S_1]$	2.66 (VEE)*
$Fl^{2-}[S_2]$	3.01 (VEE)*

In order to investigate the dissociation dynamics further, electronic structure calculations were performed on Fl^{2-}, Fl^{-} and $Fl\text{-}CO_2^{-}$. Of most importance to the decarboxylation process is the relative energetics of the $Fl^{-}[D_0]$ and $Fl^{-}[D_1]$ states compared to the dissociation asymptote $Fl\text{-}CO_2^{-} + CO_2$. The calculations indicate that $Fl^{-}[D_0]$ is bound with respect to $Fl\text{-}CO_2^{-} + CO_2$, with a bond dissociation energy of 0.82 eV. The calculated bond dissociation energy of $Fl^{-}[D_1]$ is much smaller, at 0.09 eV, which may also indicate that $Fl^{-}[D_1]$ is bound with respect to CO_2 loss, but is within the error of the calculations and comparable to the expected internal energy of anions at 298 K. Regardless, our relative energies show clearly that decarboxylation is more facile in $Fl^{-}[D_1]$ than in $Fl^{-}[D_0]$.

The larger calculated bond dissociation energy of the $Fl^{-}[D_0]$ compared with the $Fl^{-}[D_1]$ state, together with the experimental observations of competition between the formation of Fl^{-} and $Fl\text{-}CO_2^{-}$ following excitation to S_2 ($\lambda \leq 350$ nm), and of a relatively rapid dissociation (<5 μs), are consistent with the conclusion that decarboxylation is favoured following resonant tunnelling through RCB_2. Effectively, $Fl^{-}[D_1]$ lose CO_2 rapidly, whereas $Fl^{-}[D_0]$ are stable on the timescale of the experiment. The negligible bond dissociation energy for $Fl^{-}[D_1]$ suggests that loss of CO_2 is energetically possible whenever $Fl^{2-}[S_2]$ can be excited, which matches well with the observed action spectra where one-photon decarboxylation is seen for $\lambda < 350$ nm, and suggests that the potential energy surface would be, at most, weakly repulsive. A cartoon illustrating the rapid decarboxylation of $Fl^{-}[D_1]$, following its formation via tunnelling through RCB_2, is shown in Figure 6a.

ACCEPTED MANUSCRIPT
The Journal of Chemical Physics
AIP Publishing
This is the author's peer reviewed, accepted manuscript. However, the online version of record will be different from this version once it has been copyedited and typeset.
PLEASE CITE THIS ARTICLE AS DOI: 10.1063/5.0144851

However, if the above picture of dissociation was complete, we would expect to see a fixed ratio of Fl^- and $Fl\text{-}CO_2^-$ once excitation to $Fl^{2-}[S_2]$ was energetically accessible. In reality, the relative intensity of $Fl\text{-}CO_2^-$ signal compared to Fl^- increases with photon energy, as shown in figure SI3, suggesting that there is a second dissociation mechanism at play. As we have established that decarboxylation must follow electron loss via tunnelling through a RCB, we conclude that one-photon DPD must also be a possible channel from $Fl^-[D_0]$ when sufficient vibrational energy is present to overcome the bond dissociation energy. The $Fl^-[D_0]$ state is populated following resonant electron loss from $Fl^{2-}[S_1]$ and so decarboxylation becomes energetically accessible for $\lambda < 375$ nm, corresponding to the energy of $Fl^{2-}[S_1]$ plus the $Fl^-[D_0]$ dissociation energy (2.48 eV (500 nm) + 0.82 eV = 3.30 eV (375 nm)). This decarboxylation channel, shown in Figure 6b, would be expected to increase in favourability as the photon energy increases, as there is a larger likelihood of the vibrational modes relevant to decarboxylation to be populated. This decarboxylation mechanism is likely to be slower than dissociation via $Fl^-[D_1]$ and may be expected to result in a broader time-of-flight distribution for $Fl\text{-}CO_2^-$. However, low absolute signal levels make measurement of such broadened features (in a minor channel) not presently feasible, and it should be noted that a prompt (i.e. <5 μs) contribution is also present because it appears in the $Fl\text{-}CO_2^-$ signal.

In summary, one-photon decarboxylation occurs after excitation to the $Fl^{2-}[S_2]$, primarily from $Fl^-[D_1]$ produced via resonant tunnelling through RCB_2, but with a minor contribution from vibrationally excited anions produced via internal conversion from $Fl^{2-}[S_2]$ to $Fl^{2-}[S_1]$ and subsequent resonant tunnelling through RCB_1. The combination of these two mechanisms explains the observed one-photon Fl^{2-} action spectra, when combined with our knowledge of the electron dynamics from photoelectron imaging. This picture of the decarboxylation dynamics is summarised in figure 6, which provides a comprehensive view of the possible mechanisms at play following photoexcitation. This picture is also consistent with

ACCEPTED MANUSCRIPT
The Journal of Chemical Physics
AIP Publishing
This is the author's peer reviewed, accepted manuscript. However, the online version of record will be different from this version once it has been copyedited and typeset.
PLEASE CITE THIS ARTICLE AS DOI: 10.1063/5.0144851

the observations from previous CID and IR excitation experiments, where those excitation methods provided sufficient energy to surpass the $Fl^-[D_0]$ dissociation barrier after an electron has been lost.[2]

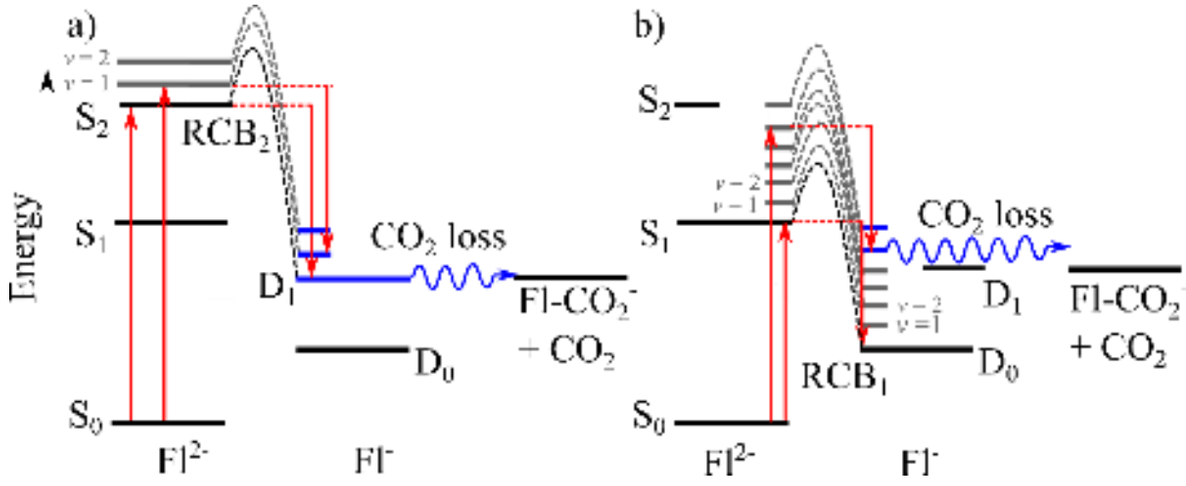

Figure 6: Cartoon of the possible decarboxylation routes following electron loss via a) resonant tunnelling through RCB_2 and rapid decarboxylation and b) resonant tunnelling through RCB_1 and slow decarboxylation for highly internally excited anions. Electronic dynamics (including photoexcitation) are shown in red with CO_2 decarboxylation dynamics in blue. Vibrational energy levels of D_0 and D_1 with sufficient energy for decarboxylation are also shown in blue.

The final consideration is the mechanism of the two-photon electron loss and decarboxylation process, which occurs in the visible region. For $\lambda \geq 400$ nm (Figure 4) electron loss results in the production of $Fl^-[D_0]$. The subsequent absorption of a second photon, which results in decarboxylation, is likely to form an electronically excited $Fl^-[D_n]$. This is supported by the observation of clear vibrational structure in the action spectrum of Fl^- (Figure 5). The $Fl^-[D_n]$ electronically excited state is higher lying than the $Fl^-[D_1]$ state, which lies 0.73 eV above $Fl^-[D_0]$ (see Table 1) and may be dissociative along the CO_2 coordinate. Alternatively, decarboxylation could take place following internal conversion to the weakly-bound $Fl^-[D_1]$ state or from the $Fl^-[D_0]$, although this would be a statistical and slower dissociation mechanism.

ACCEPTED MANUSCRIPT
The Journal of Chemical Physics
AIP Publishing
This is the author's peer reviewed, accepted manuscript. However, the online version of record will be different from this version once it has been copyedited and typeset.
PLEASE CITE THIS ARTICLE AS DOI: 10.1063/5.0144851

V. Conclusions

A new reflectron secondary mass spectrometer has been used to record the action spectra of the photodetachment and DPD product channels, following irradiation of Fl^{2-} at wavelengths between 260 and 600 nm. The action spectrum of Fl^{2-}, recorded by monitoring Fl^-, indicates that at least two excited states of Fl^{2-} are observed. In addition, photoelectron imaging demonstrates the presence of electron loss via several distinct resonant tunnelling channels, through different RCBs. For $\lambda > 400$ nm, excitation to the $Fl^{2-}[S_1]$ results in photodetachment, with CO_2 loss only occurring via a two-photon process of photodetachment and subsequent decarboxylation of Fl^-. For $\lambda < 400$ nm, CO_2 loss occurs via a one photon process, with increasing relative yields of $Fl\text{-}CO_2^-$ as the photon energy increases. In addition, electronic structure calculations indicate that $Fl^-[D_0]$ is bound with respect to decarboxylation, whereas $Fl^-[D_1]$ is similar in energy to the dissociation asymptote. Taken together, these observations indicate that decarboxylation occurs rapidly following tunnelling through RCB_2 and formation of a $Fl^-[D_1]$, with a smaller contribution from the formation of highly vibrationally excited $Fl^-[D_0]$ following tunnelling through RCB_1. Finally, the two-photon process of electron loss, via direct detachment or tunnelling through RCB_1, and subsequent decarboxylation, which is observed in the visible region, is likely mediated by a high-lying repulsive state of Fl^-.

Supplementary Material

The supplementary material contains an example time-of-flight trace, a low laser power fragment action spectrum of Fl^{2-} and a plot showing the proportion of decarboxylation as a function of wavelength.

Acknowledgements

Jemma A. Gibbard is thankful for the support of a Ramsay Memorial Fellowship. The authors would like to thank Adam Mendoza for developing the data acquisition program used to record the action spectra in this work.

Conflicts of interest

The authors have no conflicts of interest to disclose.

Data Availability

The data that support the findings of this study are available from the corresponding author upon reasonable request.

References

1. Earp, A.; Hanson, C. E.; Ralph, P. J.; Brando, V. E.; Allen, S.; Baird, M.; Clementson, L.; Daniel, P.; Dekker, A. G.; Fearns, P. R. C. S.; Parslow, J.; Strutton, P. G.; Thompson, P. A.; Underwood, M.; Weeks, S.; Doblin, M. A., Review of fluorescent standards for calibration of in situ fluorometers: Recommendations applied in coastal and ocean observing programs. *Opt. Express* **2011,** *19* (27), 26768-26782.
2. McQueen, P. D.; Sagoo, S.; Yao, H.; Jockusch, R. A., On the Intrinsic Photophysics of Fluorescein. *Ang. Chem. Int. Ed.* **2010,** *49* (48), 9193-9196.
3. Horke, D. A.; Chatterley, A. S.; Verlet, J. R. R., Effect of Internal Energy on the Repulsive Coulomb Barrier of Polyanions. *Phys. Rev. Lett.* **2012,** *108* (8), 083003.
4. Pino, G. A.; Jara-Toro, R. A.; Aranguren-Abrate, J. P.; Dedonder-Lardeux, C.; Jouvet, C., Dissociative photodetachment vs. photodissociation of aromatic carboxylates: the benzoate and naphthoate anions. *Phys. Chem. Chem. Phys.* **2019,** *21* (4), 1797-1804.
5. Gibbard, J. A.; Continetti, R. E., Photoelectron photofragment coincidence spectroscopy of carboxylates. *RSC Adv.* **2021,** *11* (54), 34250-34261.
6. Dreuw, A.; Cederbaum, L. S., Nature of the repulsive Coulomb barrier in multiply charged negative ions. *Phys. Rev. A* **2000,** *63* (1), 049904.
7. Scheller, M. K.; Compton, R. N.; Cederbaum, L. S., Gas-Phase Multiply Charged Anions. *Science* **1995,** *270* (5239), 1160-1166.
8. Dreuw, A.; Cederbaum, L. S., Multiply Charged Anions in the Gas Phase. *Chem. Rev.* **2002,** *102* (1), 181-200.
9. Kalcher, J.; Sax, A. F., Gas Phase Stabilities of Small Anions: Theory and Experiment in Cooperation. *Chem. Rev.* **1994,** *94* (8), 2291-2318.
10. Boldyrev, A. I.; Gutowski, M.; Simons, J., Small Multiply Charged Anions as Building Blocks in Chemistry. *Acc. Chem. Res.* **1996,** *29* (10), 497-502.
11. Simons, J., Molecular Anions. *J. Phys. Chem. A* **2008,** *112* (29), 6401-6511.
12. Gibbard, J. A.; Verlet, J. R. R., Kasha's Rule and Koopmans' Correlations for Electron Tunnelling through Repulsive Coulomb Barriers in a Polyanion. *J. Phys. Chem. Lett.* **2022,** *13* (33), 7797 - 7801.

ACCEPTED MANUSCRIPT
The Journal of Chemical Physics
AIP Publishing
This is the author's peer reviewed, accepted manuscript. However, the online version of record will be different from this version once it has been copyedited and typeset.
PLEASE CITE THIS ARTICLE AS DOI: 10.1063/5.0144851

ACCEPTED MANUSCRIPT
The Journal of Chemical Physics
AIP Publishing
This is the author's peer reviewed, accepted manuscript. However, the online version of record will be different from this version once it has been copyedited and typeset.
PLEASE CITE THIS ARTICLE AS DOI: 10.1063/5.0144851

13. Boxford, W. E.; Pearce, J. K.; Dessent, C. E. H., Ionic fragmentation versus electron detachment in isolated transition metal complex dianions. *Chem. Phys. Lett.* **2004,** *399* (4), 465-470.
14. Weis, P.; Hampe, O.; Gilb, S.; Kappes, M. M., Metastability of isolated platinum and palladium tetrahalide dianions and the role of electron tunneling. *Chem. Phys. Lett.* **2000,** *321* (5-6), 426-432.
15. Dau, P. D.; Liu, H.-T.; Yang, J.-P.; Winghart, M.-O.; Wolf, T. J. A.; Unterreiner, A.-N.; Weis, P.; Miao, Y.-R.; Ning, C.-G.; Kappes, M. M.; *et al*, Resonant tunneling through the repulsive Coulomb barrier of a quadruply charged molecular anion. *Phys. Rev. A* **2012,** *85* (6), 064503.
16. Winghart, M.-O.; Yang, J.-P.; Kühn, M.; Unterreiner, A.-N.; Wolf, T. J. A.; Dau, P. D.; Liu, H.-T.; Huang, D.-L.; Klopper, W.; Wang, L.-S.; et al, Electron tunneling from electronically excited states of isolated bisdisulizole-derived trianion chromophores following UV absorption. *Phys. Chem. Chem. Phys.* **2013,** *15* (18), 6726.
17. Winghart, M.-O.; Yang, J.-P.; Vonderach, M.; Unterreiner, A.-N.; Huang, D.-L.; Wang, L.-S.; Kruppa, S.; Riehn, C.; Kappes, M. M., Time-resolved photoelectron spectroscopy of a dinuclear Pt(II) complex: Tunneling autodetachment from both singlet and triplet excited states of a molecular dianion. *J. Chem. Phys.* **2016,** *144* (5), 054305.
18. Marcum, J. C.; Weber, J. M., Electronic photodissociation spectra and decay pathways of gas-phase $IrBr_6^{2-}$. *J. Chem. Phys.* **2009,** *131* (19), 194309.
19. Verlet, J. R. R.; Horke, D. A.; Chatterley, A. S., Excited states of multiply-charged anions probed by photoelectron imaging: riding the repulsive Coulomb barrier. *Phys. Chem. Chem. Phys.* **2014,** *16* (29), 15043-15052.
20. Wang, X.-B.; Wang, L.-S., Photoelectron Spectroscopy of Multiply Charged Anions. *Ann. Rev. Phys. Chem.* **2009,** *60* (1), 105-126.
21. Wang, X.-B.; Ding, C.-F.; Wang, L.-S., Photodetachment Spectroscopy of a Doubly Charged Anion: Direct Observation of the Repulsive Coulomb Barrier. *Phys. Rev. Lett.* **1998,** *81* (16), 3351-3354.
22. Wang, L.-S.; Ding, C.-F.; Wang, X.-B.; Nicholas, J. B., Probing the Potential Barriers and Intramolecular Electrostatic Interactions in Free Doubly Charged Anions. *Phys. Rev. Lett.* **1998,** *81* (13), 2667-2670.
23. Gibbard, J. A.; Clarke, C. J.; Verlet, J. R. R., Photoelectron spectroscopy of the protoporphyrin IX dianion. *Phys. Chem. Chem. Phys.* **2021,** *23* (34), 18425-18431.
24. Boxford, W. E.; El Ghazaly, M. O. A.; Dessent, C. E. H.; Brøndsted Nielsen, S., High-energy collision induced dissociation of iridium hexa-halide dianions: Observation of triple electron detachment and other decay pathways. *Int. J. Mass Spec.* **2005,** *244* (1), 60-64.
25. Friedrich, J.; Gilb, S.; Ehrler, O. T.; Behrendt, A.; Kappes, M. M., Electronic photodissociation spectroscopy of isolated IrX_6^{2-} (X=Cl,Br). *J. Chem. Phys.* **2002,** *117* (6), 2635-2644.
26. Marcum, J. C.; Halevi, A.; Weber, J. M., Photodamage to isolated mononucleotides—photodissociation spectra and fragment channels. *Phys. Chem. Chem. Phys.* **2009,** *11* (11), 1740.
27. Anstöter, C. S.; Bull, J. N.; Verlet, J. R. R., Ultrafast dynamics of temporary anions probed through the prism of photodetachment. *Int. Rev. Phys. Chem.* **2016,** *35* (4), 509-538.
28. Gibbard, J. A.; Castracane, E.; Shin, A. J.; Continetti, R. E., Dissociative photodetachment dynamics of the oxalate monoanion. *Phys. Chem. Chem. Phys.* **2020,** *22* (3), 1427-1436.
29. Lu, Z.; Continetti, R. E., Dynamics of the Acetyloxyl Radical Studied by Dissociative Photodetachment of the Acetate Anion. *J. Phys. Chem. A* **2004,** *108* (45), 9962-9969.
30. Gibbard, J. A.; Castracane, E.; Krylov, A. I.; Continetti, R. E., Photoelectron photofragment coincidence spectroscopy of aromatic carboxylates: benzoate and *p*-coumarate. *Phys. Chem. Chem. Phys.* **2021,** *23* (34), 18414-18424.
31. Boesl, U.; Weinkauf, R.; Schlag, E. W., Reflectron time-of-flight mass spectrometry and laser excitation for the analysis of neutrals, ionized molecules and secondary fragments. *Int. J. Mass Spec. and Ion Proc.* **1992,** *112* (2), 121-166.

ACCEPTED MANUSCRIPT
The Journal of Chemical Physics
AIP Publishing
This is the author's peer reviewed, accepted manuscript. However, the online version of record will be different from this version once it has been copyedited and typeset.
PLEASE CITE THIS ARTICLE AS DOI: 10.1063/5.0144851

32. Dessent, C. E. H.; Johnson, M. A., Photoinitiation of Gas-Phase S_N2 Reactions through the Evans−Polanyi Excited State Surface. *J. Am. Chem. Soc.* **1997,** *119* (21), 5067-5068.
33. Lecointre, J.; Roberts, G. M.; Horke, D. A.; Verlet, J. R. R., Ultrafast Relaxation Dynamics Observed Through Time-Resolved Photoelectron Angular Distributions. *J. Phys. Chem. A* **2010,** *114* (42), 11216-11224.
34. Stanley, L. H.; Anstöter, C. S.; Verlet, J. R. R., Resonances of the anthracenyl anion probed by frequency-resolved photoelectron imaging of collision-induced dissociated anthracene carboxylic acid. *Chem. Sci.* **2017,** *8* (4), 3054-3061.
35. Hirata, S.; Head-Gordon, M., Time-dependent density functional theory within the Tamm–Dancoff approximation. *Chem. Phys. Lett.* **1999,** *314* (3), 291-299.
36. Krishnan, R.; Binkley, J. S.; Seeger, R.; Pople, J. A., Self‐consistent molecular orbital methods. XX. A basis set for correlated wave functions. *J. Chem. Phys.* **1980,** *72* (1), 650-654.
37. Frisch, M. J.; Trucks, G. W.; Schlegel, H. B.; Scuseria, G. E.; Robb, M. A.; Cheeseman, J. R.; Scalmani, G.; Barone, V.; Petersson, G. A.; Nakatsuji, H.; Li, X.; Caricato, M.; Marenich, A. V.; Bloino, J.; Janesko, B. G.; Gomperts, R.; Mennucci, B.; Hratchian, H. P.; Ortiz, J. V.; Izmaylov, A. F.; Sonnenberg, J. L.; Williams; Ding, F.; Lipparini, F.; Egidi, F.; Goings, J.; Peng, B.; Petrone, A.; Henderson, T.; Ranasinghe, D.; Zakrzewski, V. G.; Gao, J.; Rega, N.; Zheng, G.; Liang, W.; Hada, M.; Ehara, M.; Toyota, K.; Fukuda, R.; Hasegawa, J.; Ishida, M.; Nakajima, T.; Honda, Y.; Kitao, O.; Nakai, H.; Vreven, T.; Throssell, K.; Montgomery Jr., J. A.; Peralta, J. E.; Ogliaro, F.; Bearpark, M. J.; Heyd, J. J.; Brothers, E. N.; Kudin, K. N.; Staroverov, V. N.; Keith, T. A.; Kobayashi, R.; Normand, J.; Raghavachari, K.; Rendell, A. P.; Burant, J. C.; Iyengar, S. S.; Tomasi, J.; Cossi, M.; Millam, J. M.; Klene, M.; Adamo, C.; Cammi, R.; Ochterski, J. W.; Martin, R. L.; Morokuma, K.; Farkas, O.; Foresman, J. B.; Fox, D. J. *Gaussian 16 Rev. C.01*, Wallingford, CT, 2016.
38. West, C. W.; Bull, J. N.; Verlet, J. R. R., Charged Particle Imaging of the Deprotonated Octatrienoic Acid Anion: Evidence for a Photoinduced Cyclization Reaction. *J. Phys. Chem. Lett.* **2016,** *7* (22), 4635-4640.
39. Lammich, L.; Rajput, J.; Andersen, L. H., Photodissociation pathways of gas-phase photoactive yellow protein chromophores. *Phys. Rev. E* **2008,** *78* (5).
40. Xing, X.-P.; Wang, X.-B.; Wang, L.-S., Photoelectron Imaging of Doubly Charged Anions, $^{-}O_2C(CH_2)_nCO_2^{-}$ (n = 2−8): Observation of Near 0 eV Electrons Due to Secondary Dissociative Autodetachment. *J. Phys. Chem. A* **2010,** *114* (13), 4524-4530.
41. Compton, R. N.; Reinhardt, P. W.; Cooper, C. D., Collisional ionization of Na, K, and Cs by CO_2, COS, and CS_2: Molecular electron affinities. *J. Chem. Phys.* **1975,** *63* (9), 3821.
42. Veys, K.; Escudero, D., Anti-Kasha Fluorescence in Molecular Entities: The Central Role of the Electron-Vibrational Coupling. *ChemRxiv*, 2022.

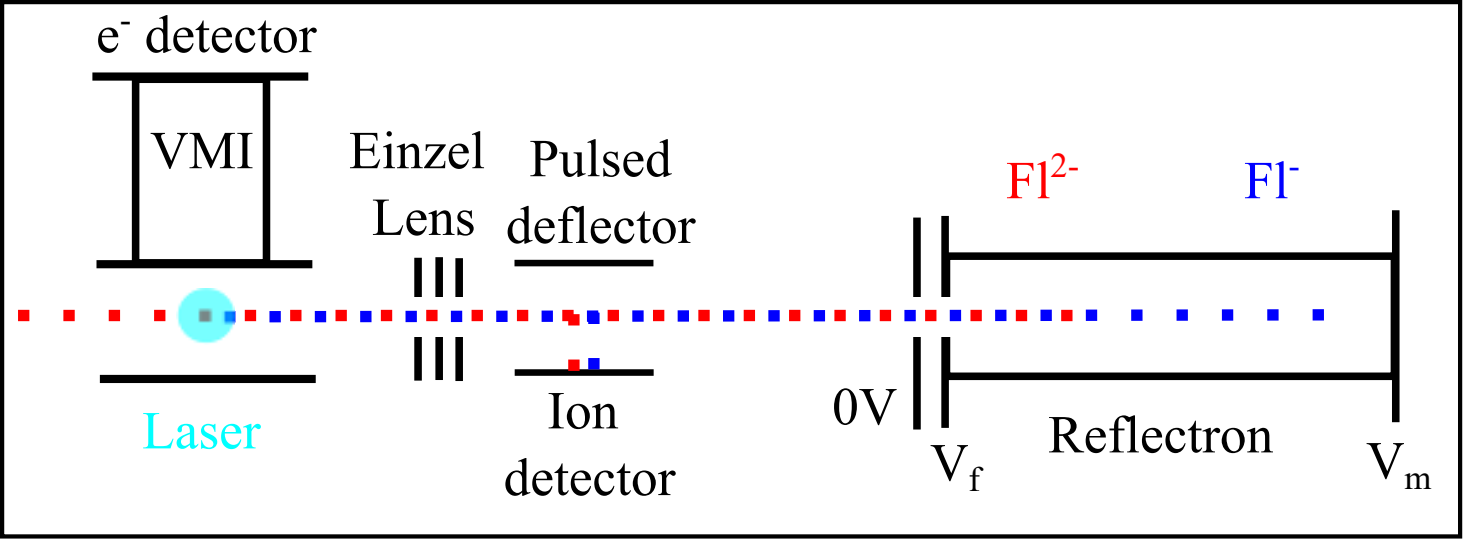
e- detector
VMI
Einzel
Lens
Pulsed
deflector
Fl2-
Fl-
Laser
Ion
detector
0V
Reflectron
Vf
Vm

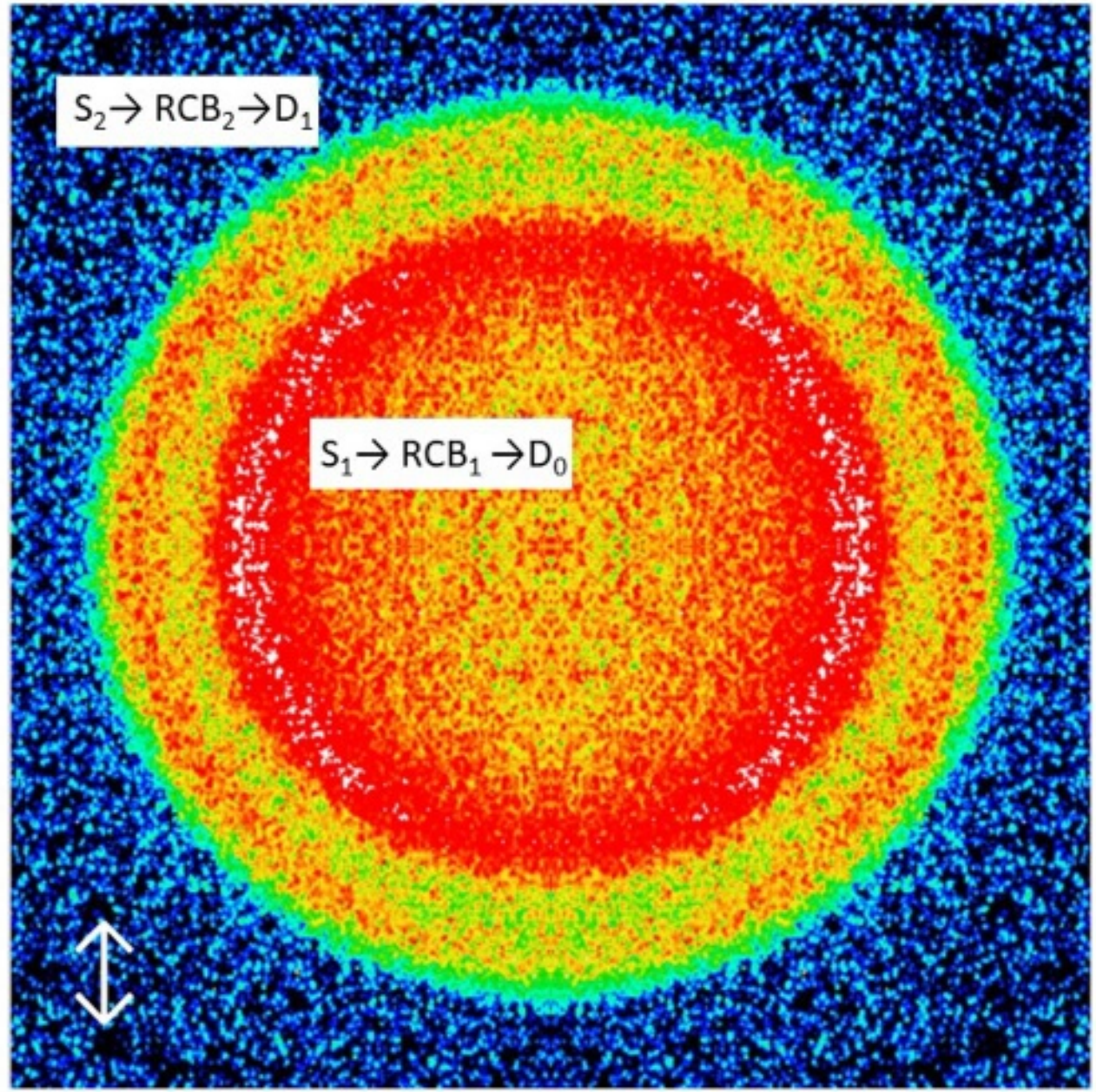
$S_2 \rightarrow RCB_2 \rightarrow D_1$
$S_1 \rightarrow RCB_1 \rightarrow D_0$

e⁻ action

Fl⁻ action

Intensity, arb. units

400 450 500 550

450 500 550 600

λ, nm

Fl-CO_2^- (m/z = 286 amu)

(x5)

UV (x3)

$S_0 \rightarrow S_2$

Fl^- (m/z = 330 amu)

Visible

$S_0 \rightarrow S_1$

Ion intensity, arb. units

300 350 400 450 500 550 600

λ, nm

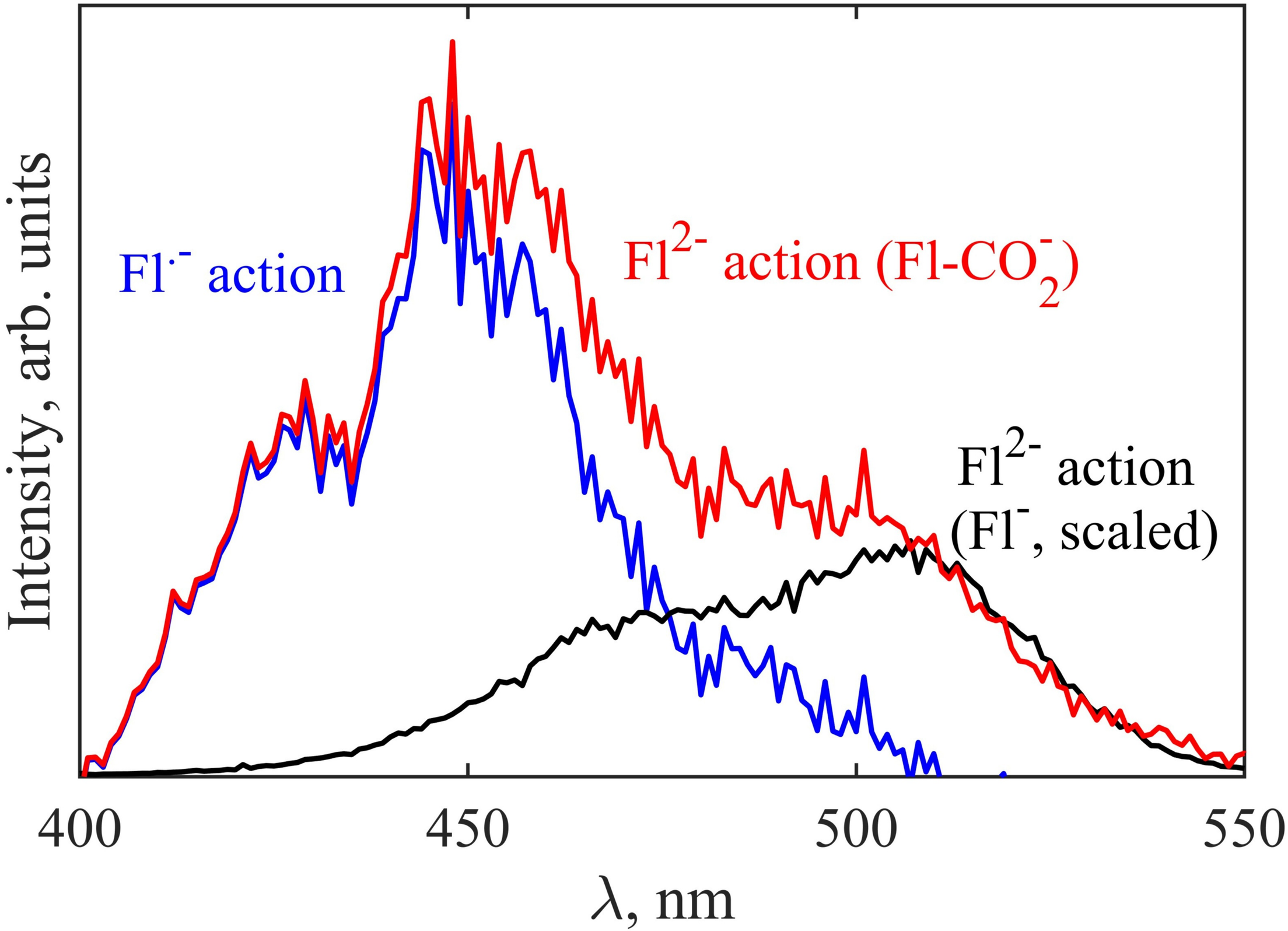
Intensity, arb. units
Fl·- action
Fl2- action (Fl-CO2-)
Fl2- action
(Fl-, scaled)
400
450
500
550
λ, nm

Accepted to J. Chem. Phys. 10.1063/5.0144851